

Figures of merit for detectors in digital radiography. II. Finite number of secondaries and structured backgrounds

Angel R. Pineda^{a)} and Harrison H. Barrett

University of Arizona, Radiology Research Building 211, 1609 North Warren, Tucson, Arizona 85724

(Received 11 June 2002; accepted for publication 16 October 2003; published 27 January 2004)

The current paradigm for evaluating detectors in digital radiography relies on Fourier methods. Fourier methods rely on a shift-invariant and statistically stationary description of the imaging system. The theoretical justification for the use of Fourier methods is based on a uniform background fluence and an infinite detector. In practice, the background fluence is not uniform and detector size is finite. We study the effect of stochastic blurring and structured backgrounds on the correlation between Fourier-based figures of merit and Hotelling detectability. A stochastic model of the blurring leads to behavior similar to what is observed by adding electronic noise to the deterministic blurring model. Background structure does away with the shift invariance. Anatomical variation makes the covariance matrix of the data less amenable to Fourier methods by introducing long-range correlations. It is desirable to have figures of merit that can account for all the sources of variation, some of which are not stationary. For such cases, we show that the commonly used figures of merit based on the discrete Fourier transform can provide an inaccurate estimate of Hotelling detectability. © 2004 American Association of Physicists in Medicine. [DOI: 10.1118/1.1631427]

Key words: image quality, lumpy background, digital radiography, DQE, NEQ

I. INTRODUCTION

Evaluation of an imaging system should be based on the performance in the task for which it was designed.¹⁻⁵ One of the tasks of interest for digital radiography is the detection of small signals. We will study how deviations from stationarity and shift invariance affect the performance of a digital detector as we vary presampling blur. In the accompanying paper,⁶ we studied the deviations for a uniform background and deterministic blurring. The three main aspects of the imaging process that we will study in this paper are the production of secondaries (electrons or light photons), structured backgrounds (patients), and random backgrounds (patient variation).

The production of secondaries is a random process where the x-ray energy is distributed into secondary light photons or electrons which in turn are detected. The location is random and number of secondaries is finite.

A flat background is a useful standard to use for evaluation of digital radiography but it does not reflect the cases of interest which are characterized by having a fluence with structure. By taking a flat background as the case to test, one makes Fourier methods more applicable but assumes that flat background results translate to those with more complicated structure. We are interested in looking at what a flat-background calculation says about a case with more complicated structure.

A more subtle source of randomness is the variation among patients. Such variation may even be the critical factor in the system performance.⁷⁻⁹ The optimization of an imaging system has to take into account the objects one is imaging. Object variation introduces long-range correlations which decrease the applicability of Fourier techniques. In

this paper, we will use a Gaussian lumpy background to introduce and study the effect of long-distance correlations in the data.

There are too many possible combinations of effects and types of Fourier techniques to study in one paper. To simplify the presentation we consider the flat background and deterministic blur as our base case and vary one component at a time. We will also only consider two implementations of Fourier methods. This approach gives us a simple way of comparing the qualitative effect of each process on lesion detectability. Researchers using Fourier methods for evaluating digital detectors^{10,11} are exploring the relation between these methods and detectability. We provide a guide as to where the assumptions used in commonly used Fourier techniques may break down in terms of predicting Hotelling detectability. How Fourier methods can be modified to better correlate with detectability measures (mathematical or psychophysical) remains a largely open question.

II. CONTINUOUS-TO-DISCRETE MODEL

A one-dimensional digital radiography system maps an x-ray point process $u(x)$ to a discrete data vector \mathbf{g} . The x rays are converted into electrons or secondary light photons. The finite number of secondaries produced are distributed randomly, and they also form a point process. The secondary point process is then discretized by the pixels. A schematic of this process is shown in Fig. 1.

The incoming x-ray Poisson point process $u(x)$ is written as

$$u(x) = \sum_{j=1}^J \delta(x - x_j), \quad (1)$$

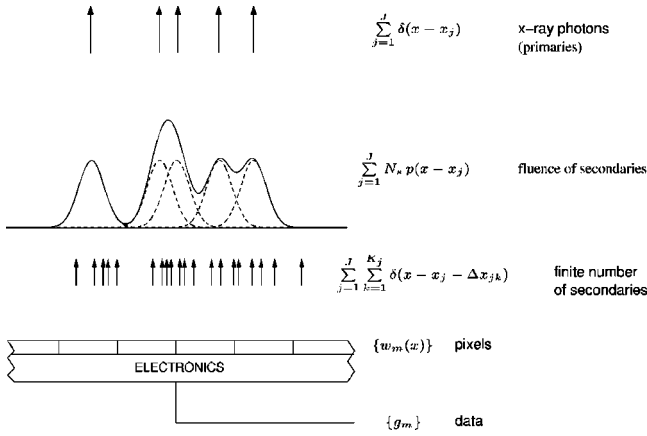


FIG. 1. Schematic of the model used for simulation. We present the case with a finite number of secondaries.

where x is the space variable (measured in units of pixels) and x_j gives the location of the j th x-ray interaction. The ensemble mean of this point process is given by $f(x)$, i.e., $\langle u(x) \rangle = f(x)$, which is called the fluence. Each of the x rays produces a random number K_j of secondaries

$$u_s(x) = \sum_{j=1}^J \sum_{k=1}^{K_j} \delta(x - x_j - \Delta x_{jk}), \quad (2)$$

where $u_s(x)$ is the secondary point process and Δx_{jk} is the difference between the location of the k th secondary from the j th x-ray interaction.

In this paper, we assume that the spatial distribution of secondaries $p(x)$ for each x-ray photon interaction is the same over the field of view and is given by a Gaussian function

$$p(x - x_j; \sigma_b) = \frac{1}{\sqrt{2\pi}\sigma_b} \exp\left(-\frac{(x - x_j)^2}{2\sigma_b^2}\right), \quad (3)$$

where σ_b is referred to as the blur width. We also assume that the mean number of secondaries $\langle K_j \rangle$ produced by each x ray is the same for all x rays, i.e., $\langle K_j \rangle = N_s$ for all j . Given these two assumptions we can express the fluence of the secondaries f_s for a given realization of the x-ray point process as

$$f_s(x) = \sum_{j=1}^J N_s p(x - x_j). \quad (4)$$

The deterministic blurring model described in the accompanying paper⁶ can be seen as the limit of a large number of secondaries. In this limit, the secondary random process can be modeled as a deterministic blurring of the x-ray point process. In the notation used in Ref. 6, $\text{blur}(x - x_j) = N_s p(x - x_j)$.

We integrate $u_s(x)$ over the pixel support $[\text{rect}(x - m)]$ and add electronic noise (n_{elec}) to get the pixel measurements g_m ,

$$\begin{aligned} g_m &= \int_{-\infty}^{\infty} \text{rect}(x - m) u_s(x) dx + [n_{\text{elec}}]_m \\ &= \int_m u_s(x) dx + [n_{\text{elec}}]_m. \end{aligned} \quad (5)$$

We use the shorthand \int_m to refer to integrating over the support of the m th pixel.

To present the various figures of merit, we write the continuous-to-discrete map as a continuous-to-continuous map followed by point sampling. The continuous (presampling) map is given by

$$\begin{aligned} g_{\text{ps}}(x) &= \sum_{j=1}^J \sum_{k=1}^{K_j} \text{rect}(x - x_j - \Delta x_{jk}) \\ &= \int_{-\infty}^{\infty} h(x - x') f(x') dx' + n_{\text{ps}}(x), \end{aligned} \quad (6)$$

where $g_{\text{ps}}(x)$ is the presampling data random process, $h(x)$ is

$$h(x) = \int_{-\infty}^{\infty} \text{rect}(x') N_s p(x - x'; \sigma_b) dx', \quad (7)$$

and n_{ps} is defined as

$$n_{\text{ps}}(x) \equiv g_{\text{ps}}(x) - \int_{-\infty}^{\infty} h(x - x') f(x) dx'. \quad (8)$$

The discrete measurements are obtained by point sampling and adding electronic noise n_{elec} ,

$$\begin{aligned} g_m &= \int_{-\infty}^{\infty} \delta(m - x) g_{\text{ps}}(x) dx + [n_{\text{elec}}]_m \\ &= g_{\text{ps}}(m) + [n_{\text{elec}}]_m, \end{aligned} \quad (9)$$

where g_m is the measurement at the m th pixel.

III. THE DETECTION TASK

We consider the task of detecting a signal in a background. The signal is deterministic, low contrast, and known; in other words, we consider the signal-known-exactly detection task where the signal does not affect the data statistics. We will consider both backgrounds known exactly and backgrounds known statistically.

The task can be seen as discriminating between the following two hypotheses:¹²⁻¹⁴

$$\mathbf{g}_0 = \mathbf{g}_b + \mathbf{n}, \quad \mathbf{g}_1 = \mathbf{g}_b + \mathbf{g}_s + \mathbf{n}, \quad (10)$$

where \mathbf{g}_i is a finite array of measurements under the i th hypothesis, and \mathbf{g}_b and \mathbf{g}_s are the components of the measurement arising from the mean background and signal, respectively, and \mathbf{n} is the noise.

The detection task is carried out by computing a test statistic t from the data and comparing it to a threshold. The signal-to-noise ratio (SNR) for any test statistic is defined as

$$\text{SNR}_t = \frac{\langle t_1 \rangle - \langle t_0 \rangle}{\sigma(t)}, \quad (11)$$

where $\langle t_i \rangle$ is the ensemble average under the i th hypothesis and $\sigma(t)$ is the standard deviation of the test statistic. The ideal observer uses the test statistic that maximizes the true positive fraction for any false positive fraction. We refer to the SNR for the ideal observer as $\text{SNR}_{\text{ideal}}$.

The signals of interest will be modeled by changes in the incoming x-ray fluence,

$$s(x; \sigma_s, l, b) = C_s(\sigma_s, b) \exp\left(-\frac{(x-l)^2}{2\sigma_s^2}\right), \quad (12)$$

where σ_s is the signal width, l is the location of the signal, and b is the background x-ray fluence. The scaling constant $C_s(\sigma_s, b)$ is chosen in two ways. The so-called SNR normalization sets $C_s(\sigma_s, b)$ so that the input $\text{SNR}_{\text{ideal}}$ is 1 as in Refs. 6 and 13 or equivalently, divides by the input SNR,

$$\text{SNR}^2 = \frac{\text{SNR}_{\text{output}}^2}{\text{SNR}^2(\text{ideal})_{\text{input}}}. \quad (13)$$

This normalization varies the amplitude of the signal as the size or location of the signal varies. Unless specifically stated, plots are SNR-normalized.

The other normalization used fixes the area under the Gaussian (AUG-normalized) to give a $\text{SNR}(\text{Hot})$ (defined in Sec. IV) of 1 in the data for a small signal with no blur. In that case, $C_s(b)$ is not a function of the signal size. This normalization will be useful when looking at structured backgrounds. We give a description of the backgrounds in their corresponding sections.

IV. SNR COMPUTATIONS

Using the mean and covariance matrix of the data, we can define the Hotelling observer,^{4,12,14,15}

$$t_{\text{Hot}}(\mathbf{g}) = \mathbf{g}_s \mathbf{K}_g^{-1} \mathbf{g}, \quad (14)$$

where \mathbf{K}_g^{-1} is the inverse of the data covariance matrix. In the nonrandom background case with deterministic blur, the Hotelling observer is the ideal observer.^{4,6} For the cases with a finite number of secondaries or random backgrounds, the Hotelling observer is the optimal linear observer³ in the sense that it maximizes SNR_t among all linear observers.

We compute the performance of the Hotelling observer for a signal at location l as

$$\text{SNR}^2(\text{Hot}, l) = \mathbf{g}_s \mathbf{K}_g^{-1} \mathbf{g}_s. \quad (15)$$

To obtain an expression that is independent of the signal location, we average over locations within a pixel, so

$$\langle \text{SNR}^2(\text{Hot}) \rangle_{\text{loc}} = \frac{1}{N_L} \sum_{i=1}^{N_L} \text{SNR}^2(\text{Hot}, l_i), \quad (16)$$

where N_L is the number of signals used to compute the average. In this paper $N_L = 100$.

In order to compute the Fourier-based figures of merit, we define the presampling modulation transfer function (PSMTF) by

$$\text{PSMTF}(\nu) = \frac{|H(\nu)|}{G}, \quad (17)$$

where $H(\nu)$ is the Fourier transform of $h(x)$ and G is $|H(0)|$. We define the digital NEQ (NEQ_{dig}) for a flat background by sampling PSMTF at the frequencies estimated from the pixel values:⁶

$$\text{NEQ}_{\text{dig}}(\text{PSMTF}) = \frac{b_0^2 G^2 \text{PSMTF}^2(\nu_i)}{\text{NPS}_{\text{dig}}(\nu_i)}, \quad (18)$$

where b_0 is the background x-ray fluence and NPS_{dig} is the variance of the DFT coefficients of the data. The DQE is a normalized version of NEQ,^{16,17}

$$\text{DQE}_{\text{dig}}(\nu_i) = \frac{\text{NEQ}_{\text{dig}}(\nu_i)}{b_0}. \quad (19)$$

To rank or optimize digital detectors we need to reduce $\text{NEQ}_{\text{dig}}(\nu)$ to a scalar. We create a SNR by defining a fractional signal $s_0(x) = s(x)/b_0$ and adding the elements of the $\text{NEQ}_{\text{dig}}(\nu)$ weighted by the frequency components of the signal of interest,

$$\text{SNR}^2(\text{DFT}, S_0) = \sum_{\nu_m = -1/2}^{1/2 - 1/M} \text{NEQ}_{\text{dig}}(\nu_m) |S_0(\nu_m)|^2, \quad (20)$$

where M is the number of detector pixels ($M = 256$ in this paper) and $S_0(\nu)$ is the Fourier transform of $s_0(x)$.

A different type of NEQ_{dig} -based SNR uses a discrete-space Fourier transform (DSFT) to estimate $\langle \text{SNR}^2(\text{Hot}) \rangle_{\text{loc}}$. We approximate the DSFT using the DFT and use the periodicity of both the DFT and DSFT,¹⁰

$$\text{SNR}^2(\text{DSFT}, S_0) = \sum_{\nu_m = -\infty}^{\infty} \text{NEQ}_{\text{dig}}(\nu_m) |S_0(\nu_m)|^2. \quad (21)$$

In all of our formulations for the SNR we assume that we have access to the mean data and the covariance matrix but not the model that generated the data. For a detailed derivation of these expressions and their relation to continuous radiography see the accompanying paper.⁶

V. THE DATA COVARIANCE MATRIX

Our approach to quantifying detectability is based on the Hotelling observer which uses only the mean and the covariance of the data. It behooves us to examine how the different sources of variation contribute to the data covariance matrix.

We can write the overall data covariance for a digital radiography system as¹⁸

$$K_g = K_g^{\text{elec}} + K_g^x + K_g^{\text{gain}} + K_g^{\text{obj}} + K_g^{K_x}, \quad (22)$$

where the terms represent, respectively, the electronic noise; the Poisson statistics of the x rays as reflected through the gain mechanism; the excess noise of the gain mechanism; the effect of the object randomness, and the effect of the re-absorbed Compton-scattered photons and K x rays.

In the accompanying paper⁶ we introduced the general approach of studying how Fourier-based methods correlate with signal detectability. We examined the effect of electronic noise and excess noise of a uniform background with

deterministic blurring. In this paper, we look at the effect of a nonuniform background and object randomness. We will account for the statistics of the gain mechanism by allowing the x-ray photons to produce a finite number of randomly located secondaries.

The re-absorption of Compton-scattered photons or K x rays creates short-distance correlations that, while they should be taken into account for realistic modeling, will not produce qualitatively different behavior than presampling blur.

VI. FINITE NUMBER OF SECONDARIES

The x-ray photons in digital radiography are detected through their interaction with the detector material. In scintillating detectors, they produce light photons. For semiconductor detector they produce electron–hole pairs. The number of secondaries and the position of the secondaries is random. We assume for simplicity that the gain process obeys Poisson statistics.

With a constant background x-ray fluence [$b(x) = b_0$] and a finite number of secondaries with mean N_s , the data covariance matrix is^{4,19}

$$[K_g]_{mm'} = \left[\int_m dx [\mathcal{H}_1 b_0](x) \right] \delta_{mm'} + \int_m dx \int_{m'} dx' [\mathcal{H}_2 b_0](x, x'), \quad (23)$$

with

$$[\mathcal{H}_1 b](x) = \int_{-\infty}^{\infty} dy N_s p(x-y) b(y)$$

and

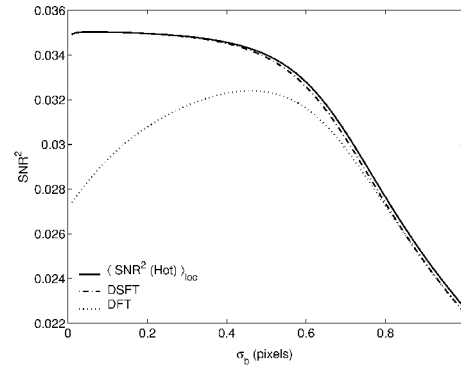
$$[\mathcal{H}_2 b](x, x') = \int_{-\infty}^{\infty} dy N_s^2 p(x-y) p(x'-y) b(y).$$

Including the random nature of the secondaries introduces a diagonal term to the data the covariance matrix. In Fig. 2, we see that for small signals, the detectability decreases as we increase the presampling blur. For larger signals, we see the same kind of maximum seen in the presence of electronic noise with deterministic blur.⁶

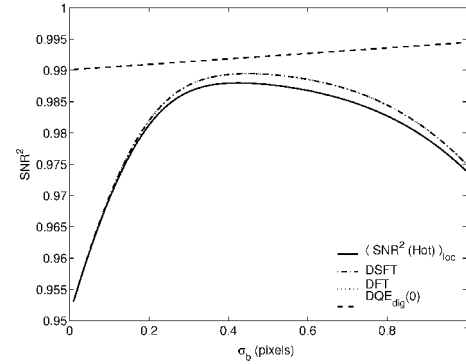
VII. NONRANDOM STRUCTURED BACKGROUNDS

For most medical cases there is anatomical structure that affects the detection task. We may consider this structure to be a nonrandom spatial function for repeated imaging of the same patient, or we can consider it to be random for different patients. Even deterministic variation in the background fluence does away with the assumption that the system can be shift invariant or stationary.

We consider a nonuniform background with deterministic blur (the limit of large number of secondaries) and no electronic noise. The covariance matrix under these circumstances is given by



(a) Small Signal ($\sigma_s = 0.01$ pixels)



(b) Large Signal ($\sigma_s = 1.0$ pixel)

FIG. 2. SNR^2 vs presampling blur for (a) a small signal and (b) a large signal. We consider the incoming photons as a Poisson point process with the mean number of secondaries (N_s) equal to 100. The increase in $\text{DQE}_{\text{dig}}(0)$ is due to the finite size of the detector.

$$[K_g]_{mm'} = \int_m dx \int_{m'} dx' [\mathcal{H}_2 b](x, x'). \quad (24)$$

We now do a numerical integration for every element of the matrix. In the limit of a large number of secondaries $\text{SNR}^2(\text{Hot})$ is independent of N_s .

To illustrate the effect of background structure, we give $b(x)$ a simple functional form

$$b(x) = b_{\min} + 4(b_{\max} - b_{\min}) \frac{x^2}{M^2}, \quad (25)$$

with $b_{\max} = 10^6$ photons/pixel and $b_{\min} = 10^5$ photons/pixel. Using this functional form (Fig. 3) for a subregion of the detector, we show how the detectability varies with the location of the signal (Fig. 3). For a small signal where we fix the amplitude (AUG-normalized), there are two sources of spatial dependence (Fig. 3). We can see the location dependence due to the pixelization and the change in detectability due to the structured background. As we would imagine, the detectability is higher for the locations with higher fluence. When we normalize by the input SNR (Fig. 3) only the pixel variability is left since we accounted for the background variation in the normalization.

For a structured background and no presampling blur, the covariance matrix is diagonal but not a multiple of the unit matrix. Taking the DFT of the data under these circum-

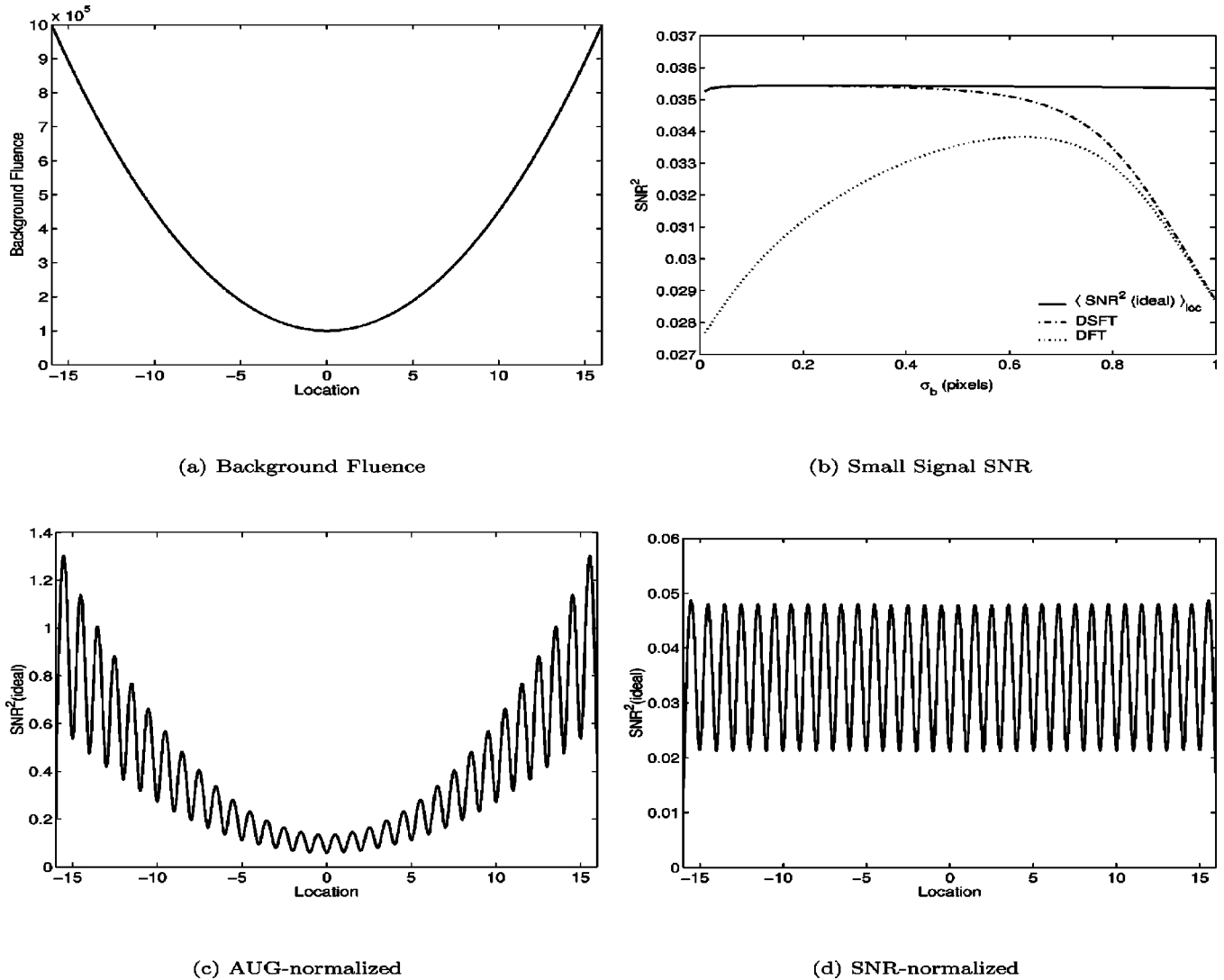


FIG. 3. A subregion of a structured background (a) and SNR dependence on blur for a small signal at the center of the domain (b). The comparison in (b) was done for the $\langle \text{SNR}^2(\text{ideal}) \rangle_{\text{loc}}$ with the structured background and the DFT-based SNRs with a flat background with the correct background value. The dependence of SNR for a small signal ($\sigma_s = 0.01$ pixels, $\sigma_b = 0.25$ pixels,) when normalized by the area under the Gaussian signal (AUG)—Ref. 12—behaves as we would expect (c). When we normalized by the input SNR, the output SNR(Hot) is independent of fluence (d).

stances takes a diagonal covariance matrix in the pixel domain to a nondiagonal matrix in the Fourier domain. The detailed computations are given in the Appendix.

VIII. RANDOM STRUCTURED BACKGROUNDS

Optimizing an imaging system for a specific object does not necessarily translate to optimizing the system for all the objects of interest. In particular, the statistics of the objects may drastically change the optimal design.^{7,8} For digital radiography, object variations introduce long-range correlations which provide an added complication to the use of Fourier-based methods. Increasing the correlation length in the data makes the covariance matrix less circulant, therefore increasing the error involved with assuming that the DFT diagonalizes the covariance matrix.

To introduce object variation, we will add a zero-mean random (lumpy) background to the flat background (with

fluence b_0). We create the backgrounds by filtering white noise such that the noise power spectrum is given by²⁰

$$W_a(\nu) = W(\nu)|A(\nu)|^2, \tag{26}$$

where by definition the power spectrum of white noise $W(\nu)$ is constant, and $A(\nu)$ is a Gaussian filter of the form

$$A(\nu) = A(0)\exp(-2\pi^2\sigma_a^2\nu^2). \tag{27}$$

Hence, the power spectrum of the lumpy background is given by

$$W_a(\nu) = W_a(0)\exp(-4\pi^2\sigma_a^2\nu^2),$$

where $W_a(0) = W(0)A(0)^2$.

To compute the data covariance matrix, we use the auto-correlation function given by the inverse Fourier transform of the power spectrum

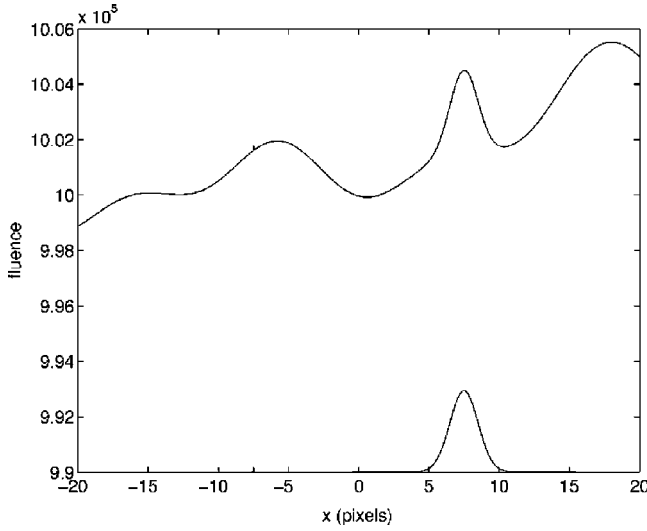


FIG. 4. Piece of a sample random background ($b_0=10^6$ photons/pixel, $W_a(0)=10^8$ photons²/pixel and $\sigma_{\text{lb}g}=5.0$ pixels). We also include the two lesions (at $x=-7.5$ and 7.5) with their amplitudes normalized to have $\text{SNR}_{\text{input}}=1$. Note that the amplitude of the signal at $x=-7.5$ is much smaller since it is easier to detect a signal with a width much smaller than the background variations.

$$R_a(x) = \frac{W_a(0)}{\sqrt{2\pi}\sigma_{\text{lb}g}} \exp\left(-\frac{x^2}{2\sigma_{\text{lb}g}^2}\right), \quad (28)$$

with $\sigma_{\text{lb}g}$ equal to $\sqrt{2}\sigma_a$. The covariance matrix of the data (with deterministic blurring and no electronic noise) when we include object randomness is given by^{4,19}

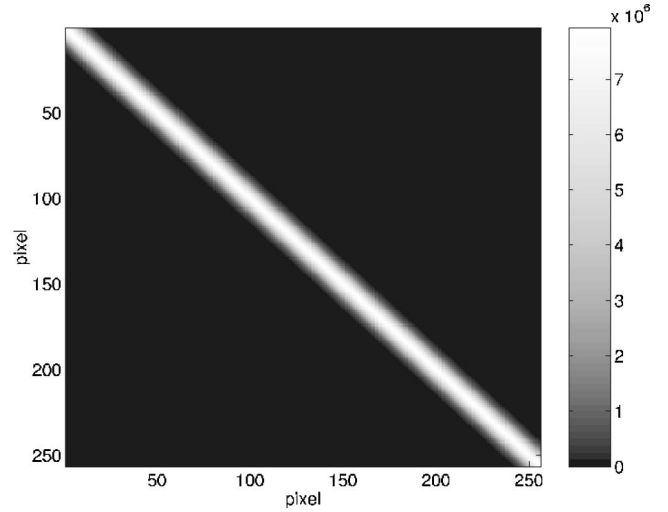
$$[K_g]_{mm'} = \int_m dx \int_{m'} dx' \{ [\mathcal{H}_2 b](x, x') + [\mathcal{H}_1 R_a \mathcal{H}_1^t](x, x') \}. \quad (29)$$

The computations were done with $b_0=10^6$ photons/pixel, $W_a(0)=10^8$ photons²/pixel and $\sigma_{\text{lb}g}=5.0$ pixels. We do not need individual realizations to compute the figures of merit but we present a sample background and lesions to better visualize the detection problem (Fig. 4).

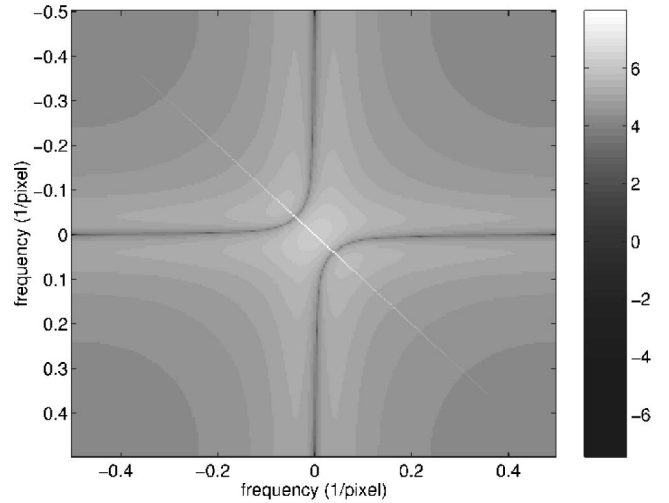
By introducing anatomical correlations, we make the covariance matrix less circulant. For $\sigma_b=1.0$ pixel, we can see that the covariance matrix has significant off-diagonal elements that propagate into the covariance of the DFT of the data (K_{DFT}) (Fig. 5). In the accompanying paper⁶ we include a similar image in the absence of anatomical variation.

The long-range correlations in the data cause a larger error in the Fourier-based methods (Fig. 6) than when there are only short-range correlations. The $\langle \text{SNR}^2(\text{Hot}) \rangle_{\text{loc}}$ remains unchanged as we increase the presampling blur because the Hotelling observer can undo the correlations caused by the lumpiness. The $\text{DQE}(0)$ is $b_0/W_a(0)$ and remains constant as we increase presampling blur. We computed $\text{SNR}_{\text{input}}$ including the lumpy background variation using numerical integration in the Fourier domain

$$\text{SNR}^2(\text{ideal})_{\text{input}} = \int_{-\infty}^{\infty} dv \frac{|S(v)|^2}{W_a(v) + b_0}. \quad (30)$$



(a) K_g (Lumpy Background)



(b) $\log(|K_{\text{DFT}}|)$

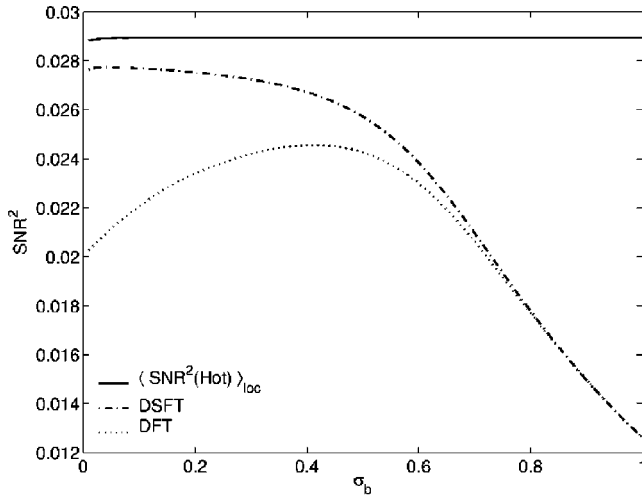
FIG. 5. (a) Covariance matrix of data with random background ($b_0=10^6$ photons/pixel, $W_a(0)=10^8$ photons²/pixel and $\sigma_{\text{lb}g}=5.0$ pixels) and $\sigma_b=1.0$ pixel. (b) Log of the covariance matrix of the DFT coefficients of data with random background and $\sigma_b=1.0$ pixel. The varying anatomical background introduces long-range correlations in the covariance matrix. Even though the background is stationary, these correlations translate to larger off-diagonal elements in the covariance matrix for the DFT coefficients (K_{DFT}) than in the flat background case (Ref. 6).

Note that because of this normalization, the SNR in the data can be 1 even in the presence of anatomical variation.

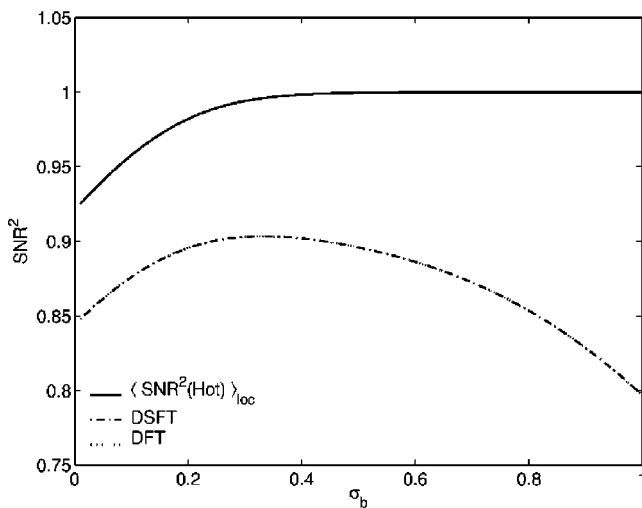
IX. DISCUSSION

The effect of the random number of secondaries on the second-order statistics of the data is an additional diagonal term to the covariance matrix. Hence the behavior of the detectability is similar when electronic noise is added to the model with deterministic blur.

If the background fluence has structure and we are concerned with quantification of the detectability of a signal, we cannot assume a constant background. Fourier methods give



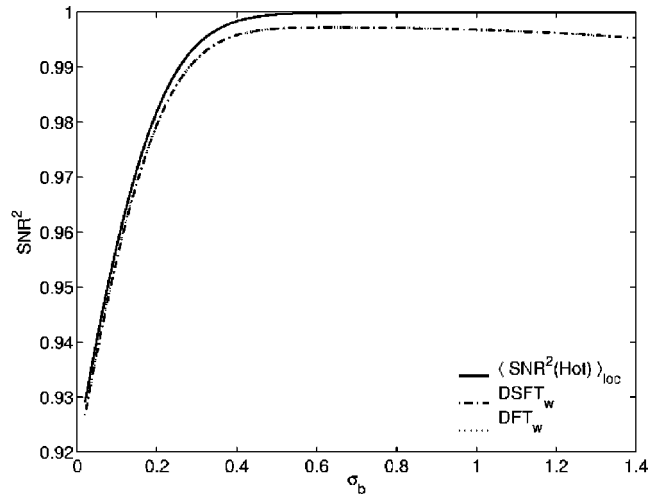
(a) Small Signal ($\sigma_s = 0.01$ pixels)



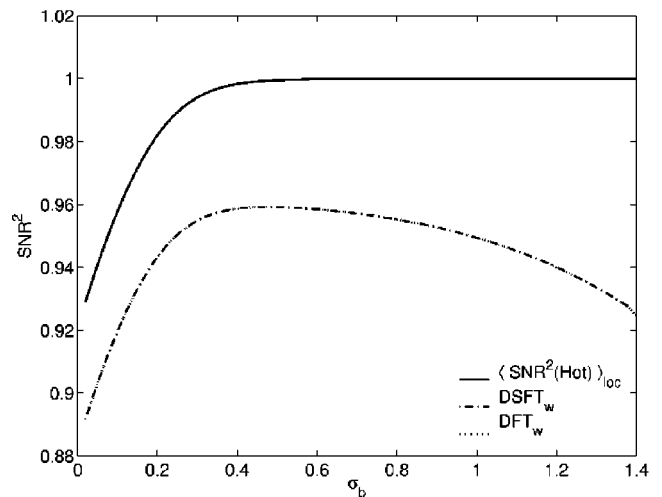
(b) Large Signal ($\sigma_s = 1.0$ pixel)

FIG. 6. SNR^2 vs presampling blur with a random (lumpy) background ($b_0 = 10^6$ photons/pixel, $W_a(0) = 10^8$ photons²/pixel and $\sigma_{\text{bkg}} = 5.0$ pixels) for (a) a small signal and (b) a large signal. The correlations introduced by anatomical variation lead to quantitative differences between the SNR defined by the DSFT and SNR(Hot). We also see that the large signal is more affected than the small signal. $\text{DQE}_{\text{dig}}(0) \approx b_0/W_a(0)$ and remains constant. For this reason, $\text{DQE}_{\text{dig}}(0)$ is not included in the plot. Note that for the large signal, the DSFT and DFT plots overlap.

an inaccurate result. Fourier techniques are not localized in space, so a spatially varying fluence makes estimation of an accurate NPS_{dig} impossible. In practice, NPS_{dig} is measured with images obtained from a uniform x-ray exposure and contain much less variation than clinical images. If we are looking for a design decision, we are concerned only with relative values of the figure of merit with respect to the parameter of interest. We compute the $\text{SNR}^2(\text{ideal})$ of signals for a given position with the full covariance matrix and NEQ_{dig} -based SNRs using a flat background with the correct background value (Fig. 3). The kind of errors one gets for this comparison are similar to those obtained from a flat background.⁶ Those errors depend on the size of the detector,¹² type of spectral estimation,^{21,22} and whether one



(a) Figure 6(b) using the Hann window



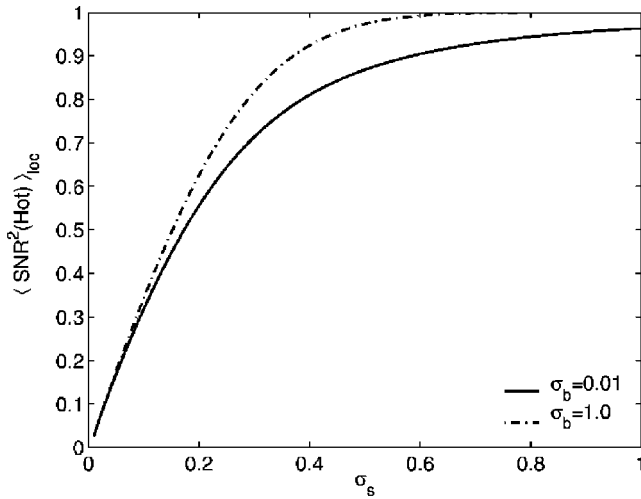
(b) Figure 6(b) using the Hann window and $M=64$

FIG. 7. We recomputed the plot from Fig. 6(b) using the Hann window for the estimation of the NPS_{dig} . In (a) we see a large effect in how the Fourier methods correlate with Hotelling detectability. Using $M=64$, (b) shows that the effect of the window will depend on the size of the images used. The “w” subscript means that the quantity was computed using the Hann window. Note that blur range goes up to 1.4.

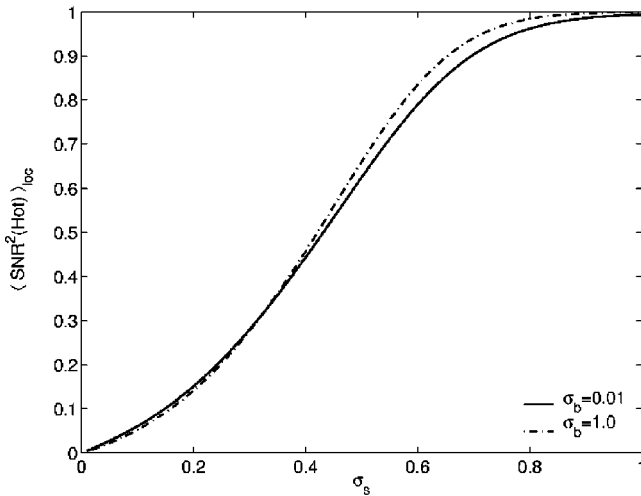
uses the analytic model that generated the data.^{10,15}

The introduction of the lumpy background affected not only the difference between NEQ_{dig} -based methods and $\text{SNR}(\text{Hot})$ for a given signal but it also increased the difference between SNRs for signals of different sizes. In the flat background cases, the deviations between $\text{SNR}(\text{Hot})$ and $\text{SNR}(\text{DSFT})$ occurred mostly for the smaller signals. When we include anatomical variation, the larger signals are also affected. Using the flat-background result in Ref. 6, we see that the large-signal detectability is more affected by the background randomness than the small-signal detectability (Fig. 6). This is reasonable considering that the large signal is closer to the scale of the background variation.

We applied the Hann window²³ to the estimation of the NPS_{dig} . This modification resulted in a significant increase



(a) $\sigma_{\text{lb}} = 0.01$ pixels, $W_a(0) = 10^8$ photons²/pixel



(b) $\sigma_{\text{lb}} = 1.0$ pixel, $W_a(0) = 10^8$ photons²/pixel

FIG. 8. SNR^2 vs signal width for a random (lumpy) background with (a) $\sigma_{\text{lb}} = 0.01$ pixels, $W_a(0) = 10^8$ photons²/pixel and (b) $\sigma_{\text{lb}} = 1.0$ pixel, $W_a(0) = 10^8$ photons²/pixel. In the first plot, the correlation length of the background is similar to the small signal. The presampling blur separates the signal from the background. In the second plot, there is a transition. For smaller signals no blur is preferable but the opposite is true for larger signals. To emphasize smaller signals we plot SNR vs σ_b as in Ref. 13 instead of SNR vs $1/\sigma_b$ as in (Ref. 6).

in the correlation of the Fourier techniques with the Hotelling detectability as was seen in the accompanying paper.⁶ Figure 7 reproduces Fig. 6 using the Hann window instead of the implicit rect window. While the Hann window reduces the effects of a finite detector size, using $M = 64$, Fig. 7 shows that the correlation of Fourier methods with detectability will depend on the window size.

To explore the effect of the background variation on signal size we plot $\langle \text{SNR}^2(\text{Hot}) \rangle_{\text{loc}}$ vs σ_s (Fig. 8). In the first plot, the correlation length of the background is similar to the small signal. The presampling blur separates the signal from the background. In the second plot, there is a transition. For smaller signals no blur is preferable, but the opposite is true

for larger signals. The different types of behavior seen for signals shows the need to characterize both the signal and background to evaluate the detector.

X. CONCLUSIONS

The NEQ_{dig} -based approach to image quality is constrained by its stationarity and shift-invariance assumptions. While these assumptions are a sensible first model to examine, fundamentally different behavior appears when we include other sources of variation like structured and varying backgrounds. Even though we used stationary backgrounds, the finite detector size was enough to introduce significant errors in the DFT-based SNRs. As we use more complicated models, we are required to consider detectors whose impulse response is shift-variant and whose statistics are not stationary. It is important to quantify the errors involved with the use of Fourier methods as they can lead to design decisions which do not correlate with detectability.

ACKNOWLEDGMENTS

The authors would like to thank K. J. Myers and E. Clarkson for scintillating (and semiconducting) conversations. This work was made possible by funding from NIH Grant Nos. RO1 CA52643 and P41 RR14303.

APPENDIX

We consider a special case that illustrates a possible drawback of working in the Fourier domain. The intended advantage of working in the Fourier domain is a dimensionality reduction of the covariance matrix of the data. If the DFT diagonalized the $M \times M$ data covariance matrix, then the M elements of the diagonal would fully describe K_{DFT} . Let us consider the case where the background is flat and there is no presampling blur but with pixel-dependent gain (equivalently, a structured background). In that case, K_g is given by

$$[K_g]_{mm'} = \sigma_m^2 \delta_{mm'}, \quad (\text{A1})$$

where σ_m^2 is the variance at the m th pixel. The covariance matrix is diagonal in the pixel domain. If we apply the unitary DFT (D) to the data, then the covariance matrix for the DFT coefficients is

$$[K_{\text{DFT}}]_{kk'} = [DK_g D^\dagger]_{kk'} \quad (\text{A2})$$

$$= \frac{1}{M} \sum_{m=1}^M e^{2\pi i(k-k')m} \sigma_m^2. \quad (\text{A3})$$

We get a covariance matrix that is circulant in the DFT domain!

^{a)}Author to whom correspondence should be addressed; present address: Department of Radiology, Lucas MRS Center, Stanford University, Stanford, CA 94305-5488; electronic mail: pineda@stanford.edu

¹H. H. Barrett, "Objective assessment of image quality: Effects of quantum noise and object variability," J. Opt. Soc. Am. A **7**, 1266–1278 (1990).

²H. H. Barrett, J. L. Denny, R. F. Wagner, and K. J. Myers, "Objective assessment of image quality. II. Fisher information, Fourier crosstalk, and figures of merit for task performance," J. Opt. Soc. Am. A **12**, 834–852 (1995).

- ³H. H. Barrett, C. K. Abbey, and E. Clarkson, "Objective assessment of image quality. III. ROC metrics, ideal observers, and likelihood-generating functions," *J. Opt. Soc. Am. A* **15**, 1520–1534 (1998).
- ⁴H. H. Barrett and K. J. Myers, *Foundations of Image Science* (Wiley, New York, 2004).
- ⁵R. F. Wagner and D. G. Brown, "Unified SNR analysis of medical imaging systems," *Phys. Med. Biol.* **30**, 489–518 (1985).
- ⁶A. R. Pineda and H. H. Barrett, "Figures of merit for detectors in digital radiography. I. Flat background and deterministic blurring," *Med. Phys.* **31**, 348–358 (2004).
- ⁷A. E. Burgess, F. L. Jacobson, and P. F. Judy, "Lesion detection in digital mammograms," *Proc. SPIE* **4320**, 555–560 (2001).
- ⁸K. J. Myers, J. P. Rolland, H. H. Barrett, and R. F. Wagner, "Aperture optimization for emission imaging: Effect of a spatially varying background," *J. Opt. Soc. Am. A* **7**, 1279–1293 (1990).
- ⁹J. P. Rolland and H. H. Barrett, "Effect of random background inhomogeneity on observer detection performance," *J. Opt. Soc. Am. A* **9**, 649–658 (1992).
- ¹⁰M. Albert and D. A. Maidment, "Linear response theory for detectors consisting of discrete arrays," *Med. Phys.* **27**, 2417–2434 (2000).
- ¹¹J. H. Siewerdsen and D. A. Jaffray, "Optimization of x-ray imaging geometry (with application to flat-panel cone-beam computed tomography)," *Med. Phys.* **27**, 1903–1914 (2000).
- ¹²A. R. Pineda and H. H. Barrett, "What does DQE say about lesion detectability in digital radiography?" *Proc. SPIE* **4320**, 561–569 (2001).
- ¹³R. M. Gagne, J. S. Boswell, K. J. Myers, and G. Peter, "Signal detectability in digital radiography," *Proc. SPIE* **4320**, 316–325 (2001).
- ¹⁴H. H. Barrett, J. Yao, J. Rolland, and K. J. Myers, "Model observers for assessment of image quality," *Proc. Natl. Acad. Sci. U.S.A.* **90**, 9758–9765 (1993).
- ¹⁵E. Clarkson, A. R. Pineda, and H. H. Barrett, "An analytical approximation to the Hotelling trace for digital x-ray detectors," *Proc. SPIE* **4320**, 339–349 (2001).
- ¹⁶I. Cunningham, "Applied linear systems theory," *Physics and Psychophysics*, Handbook of Medical Imaging Vol. 1, edited by J. Beutel, H. L. Kundell, and R. L. Van Metter (SPIE, Bellingham, WA, 2000).
- ¹⁷J. T. Dobbins, "Image quality metrics for digital systems," in Ref. 16.
- ¹⁸H. H. Barrett, K. J. Myers, B. Gallas, E. Clarkson, and H. Zhang, "Megalopinkophobia: Its symptoms and cures," *Proc. SPIE* **4320**, 299–307 (2001).
- ¹⁹H. H. Barrett, R. F. Wagner, and K. J. Myers, "Correlated point processes in radiological imaging," *Proc. SPIE* **3032**, 110–124 (1997).
- ²⁰J. P. Rolland, "Factors influencing lesion detection in medical imaging," Ph.D. dissertation, University of Arizona, Tucson, AZ, 1990.
- ²¹A. Papoulis, *Probability, Random Variables, and Stochastic Processes* (McGraw–Hill, New York, 1991).
- ²²S. L. Lawrence, *Digital Spectral Analysis with Applications* (Prentice–Hall, Englewood Cliffs, NJ, 1987).
- ²³A. V. Oppenheim, R. W. Schaffer, and J. R. Buck, *Discrete-Time Signal Processing* (Prentice–Hall, Englewood Cliffs, NJ, 1998).